



# Super-luminescence and spectral hole burning effect in ultra-short length Er/Yb-doped phosphate fiber

REGINA GUMENYUK,<sup>1,\*</sup> ARUN POUDEL,<sup>1</sup> THIERRY JOUAN,<sup>2</sup> CATHERINE BOUSSARD-PLÉDEL,<sup>2</sup> TAPIO NIEMI,<sup>1</sup> AND LAETICIA PETIT<sup>1</sup>

<sup>1</sup>Laboratory of Photonics, Tampere University of Technology, Tampere, FI-33101, Finland

<sup>2</sup>Equipe Verres et Céramiques, UMR-CNRS 6226, Institut des Sciences Chimiques de Rennes, Université de Rennes I, F-35042, Rennes Cedex, France

\*regina.gumenyuk@tut.fi

**Abstract:** We demonstrate super-broad luminescence over 70 nm of bandwidth and spectral hole-burning effect obtained in just a few cm of novel air-clad, highly concentrated Er/Yb-doped phosphate fiber. The fiber is drawn from preforms of glasses within the  $P_2O_5 - SrO - Na_2O$  composition. The fabrication process, thermal, structural, and optical properties of the fiber are described.

© 2017 Optical Society of America under the terms of the [OSA Open Access Publishing Agreement](#)

**OCIS codes:** (060.2410) Fibers, erbium; (160.2290) Fiber materials; (060.2270) Fiber characterization.

## References and links

1. W. J. Miniscalco, "Erbium-doped glasses for fiber amplifiers at 1500 nm," *J. Lightwave Technol.* **9**(2), 234–250 (1991).
2. M. M. Bubnov, V. N. Vechkanov, A. N. Gur'yanov, K. V. Zotov, D. S. Lipatov, M. E. Likhachev, and M. V. Yashkov, "Fabrication and optical properties of fibers with an  $Al_2O_3-P_2O_5-SiO_2$  glass core," *Inorg. Mater.* **45**, 444–449 (2009).
3. J. H. Campbell and T. I. Suratwala, "Nd-doped phosphate glasses for high-energy/high-peak-power lasers," *J. Non-Cryst. Solids* **263–264**, 318–341 (2000).
4. S. Jiang, M. J. Myers, D. L. Rhonehouse, S. J. Hamlin, J. D. Myers, U. Griebner, R. Koch, and H. Schonagel, "Ytterbium-doped phosphate laser glasses," *Proc. SPIE* **2986**, 10–15 (1997).
5. V. P. Gapontsev, S. M. Matitsin, A. A. Isineev, and V. B. Kravchenko, "Erbium glass lasers and their applications," *Opt. Laser Technol.* **14**(4), 189–196 (1982).
6. S. Jiang, M. Myers, and N. Peyghambarian, "Er<sup>3+</sup> doped phosphate glasses and lasers," *J. Non-Cryst. Solids* **239**(1–3), 143–148 (1998).
7. D. Pugliese, N. G. Boetti, J. Lousteau, E. Ceci-Ginistrelli, E. Bertone, F. Geobaldo, and D. Milanese, "Concentration quenching in an Er-doped phosphate glass for compact optical lasers and amplifiers," *J. Alloys Compd.* **657**, 678–683 (2016).
8. N. G. Boetti, G. C. Scarpignato, J. Lousteau, D. Pugliese, L. Bastard, J.-E. Broquin, and D. Milanese, "High concentration Yb-Er co-doped phosphate glass for optical fiber amplification," *J. Opt.* **17**(6), 065705 (2015).
9. T. S. Conçalves, R. J. M. Silva, M. de Oliveira, Junior., C. R. Ferrari, G. Y. Poirier, H. Eckert, and A. S. S. de Camargo, "Structure-property relations in new fluorophosphates glasses singly- and co-doped with Er<sup>3+</sup> and Yb<sup>3+</sup>," *Mater. Chem. Phys.* **157**, 45–55 (2015).
10. J. F. Phillips, T. Töpfer, H. Ebendorff-Heidepriem, D. Ehrhart, and R. Sauerbrey, "Spectroscopic and lasing properties of Er<sup>3+</sup>:Yb<sup>3+</sup>-doped fluoride phosphate glasses," *Appl. Phys. B* **72**(4), 399–405 (2001).
11. M. Sołtys, L. Żur, J. Pisarska, T. Goryczka, and W. A. Pisarski, "Selective oxide modifiers M<sub>2</sub>O<sub>3</sub> (M=Al, Ga) as crystallizing agents in Er<sup>3+</sup>-doped lead phosphate glass host," *Ceram. Int.* **41**(3), 4334–4339 (2015).
12. S. Yliniemi, S. Honkanen, A. Ianoul, A. Laronche, and J. Albert, "Photosensitivity and volume gratings in phosphate glasses for rare-earth-doped ion-exchanged optical waveguide lasers," *J. Opt. Soc. Am. B* **23**(12), 2470–2478 (2006).
13. S. Jiang, T. Luo, B. C. Hwang, F. Smekatala, K. Seneschal, J. Lucas, and N. Peyghambarian, "Er<sup>3+</sup>-doped phosphate glasses for fiber amplifiers with high gain per unit length," *J. Non-Cryst. Solids* **263**, 364–368 (2000).
14. J. C. Knowles, "Phosphate based glasses for biomedical applications," *J. Mater. Chem.* **13**, 2395–2401 (2003).
15. P. Hofmann, C. Voigtländer, S. Nolte, N. Peyghambarian, and A. Schulzgen, "550-mW output power from a narrow linewidth all-phosphate fiber laser," *J. Lightwave Technol.* **31**(5), 756–760 (2013).
16. B.-C. Hwang, S. Jiang, T. Luo, K. Seneschal, G. Sorbello, M. Morrell, F. Smekatala, S. Honkanen, J. Lucas, and N. Peyghambarian, "Performance of high-concentration Er<sup>3+</sup>-doped phosphate fiber amplifiers," *IEEE Photonics Technol. Lett.* **13**(3), 197–199 (2001).

17. Y. Hu, S. Jiang, T. Luo, K. Seneschal, M. Morrell, F. Smektala, S. Honkanen, J. Lucas, and N. Peyghambarian, "Performance of high-concentration Er<sup>3+</sup>-Yb<sup>3+</sup>-codoped phosphate fiber amplifiers," *IEEE Photonics Technol. Lett.* **13**(7), 657–659 (2001).
18. C. Y. Cho, Y. C. Chen, Y. P. Huang, Y. J. Huang, K. W. Su, and Y. F. Chen, "High-repetition-rate quasi-CW side-pumped mJ eye-safe laser with a monolithic KTP crystal for intracavity optical parametric oscillator," *Opt. Express* **22**(7), 7625–7631 (2014).
19. S. E. Stokowski, R. A. Saroyan, and M. J. Weber, "Nd-doped laser glass spectroscopic and physical properties," Lawrence Livermore National Laboratory, Rep. M-095, 1981, Rev. 2.
20. P. Lopez-Isoa, T. Salminen, T. Hakkarainen, L. Petit, D. Janner, N. G. Boetti, M. Lastusaari, D. Pugliese, P. Paturi, and D. Milanese, "Effect of partial crystallization on the structural and luminescence properties of Er<sup>3+</sup>-doped phosphate glasses," *Materials (Basel)* **10**(5), 473 (2017).
21. J. Massera, Y. Shpotyuk, F. Sabatier, T. Jouan, C. Bousard-Plédel, C. Roiland, B. Bureau, L. Petit, N. G. Boetti, D. Milanese, and L. Hupa, "Processing and characterization of novel borophosphate glasses and fibers for medical applications," *J. Non-Cryst. Solids* **425**, 52–60 (2015).
22. T. Harada, H. In, H. Takebe, and K. Morinaga, "Effect of B<sub>2</sub>O<sub>3</sub> Addition on the Thermal Stability of Barium Phosphate Glasses for Optical Fiber Devices," *J. Am. Ceram. Soc.* **87**(3), 408–411 (2004).
23. J. Massera, A. Haldeman, D. Milanese, H. Gebavi, M. Ferraris, P. Foy, W. Hawkins, J. Ballato, R. Stolen, L. Petit, and K. Richardson, "Processing and characterization of core-clad tellurite glass preforms and fibers fabricated by rotational casting," *Opt. Mater.* **32**(5), 582–588 (2010).
24. A. Poudel, I. Dmitrieva, R. Gumenyuk, L. Mihai, D. Sporea, O. Mureşan, I. Rusen, T. Hakkarainen, N. Boetti, T. Niemi, and L. Petit, "Effect of ZnO addition and of alpha particle irradiation on various properties of Er<sup>3+</sup>, Yb<sup>3+</sup> doped phosphate glasses," *Applied Science* **7**, 1094 (2017).
25. R. Francini, F. Giovenale, U. M. Grassano, P. Laporta, and S. Taccheo, "Spectroscopy of Er and Er±Yb-doped phosphate glasses," *Opt. Mater.* **13**(4), 417–425 (2000).
26. D. Creeden, H. Pretorius, J. Limongelli, and S. D. Setzler, "Single frequency 1560 nm Er:Yb fiber amplifier with 207 W output power and 50.5% slope efficiency," *Proc. SPIE* **9728**, 97282L (2016).
27. J. Zhou, F. Moshary, B. M. Gross, M. F. Arend, and S. A. Ahmed, "Population dynamics of co-doped phosphate glass," *J. Appl. Phys.* **96**(1), 237–241 (2004).
28. T. K. Subramaniam, "Erbium Doped Fiber Lasers for Long Distance Communication Using Network of Fiber Optics," *American Journal of Optics and Photonics* **3**(3), 34–37 (2015).
29. M. Eilchi and P. Parvin, "Gain saturation in optical fiber amplifiers," in *Fiber Lasers*, Chapter 13, M. Paul Ed. InTech, 2016, pp. 297–320.
30. H. Shalibeik, *Rare-earth-doped Fiber Lasers and Amplifiers* (Cuvillier Verlag, 2007).
31. P. Nandi and G. Jose, "Superfluorescence from Yb- and Yb–Er-doped phosphotellurite glass fibres," *Opt. Fiber Technol.* **14**(4), 275–280 (2008).
32. H.-Q. Shangguan and L. W. Casperson, "Estimation of scattered light on the surface of unclad optical fiber tips: a new approach," *Opt. Commun.* **152**(4–6), 307–312 (1998).

## 1. Introduction

Erbium-doped glasses keep on great interest of scientific society due to their unique ability to generate light at the wavelength of 1520 - 1570 nm, which corresponds to the intra-4f transition of Er<sup>3+</sup> from <sup>4</sup>I<sub>13/2</sub> to <sup>4</sup>I<sub>15/2</sub> [1]. This wavelength is important for a variety of applications such as telecommunications, LIDAR, spectroscopy, and bioimaging. The continuous demand in improving the existing technology encourages the development of innovative and advanced Er-based composite materials.

Silica glass has been intensively studied as a host material because of its wide wavelength range with good optical transparency, high mechanical strength against pulling and even bending as well as chemical stability. However, silica glass when doped with rare-earth (RE) ions have some limitations due to RE clustering or inappropriate RE local environment [2]. Phosphate glasses are of interest for the engineering of photonic devices due to their following properties: easy processing, good thermal stability and excellent optical characteristics, such as high transparency in the UV-Visible-Near Infrared (UV-Vis-NIR) region [3–7]. Phosphate glasses have been extensively investigated since these glasses can incorporate high amount of dopant (as opposed to silicate glasses) and, therefore, quenching phenomenon occurs in these glasses at very high concentrations of RE ions [7–9]. Additionally, they provide smooth and broad gain spectrum [10, 11]. Yb-Er-co-doped phosphate glasses are characterized also by reasonably high photosensitivity, what gives an opportunity to design effective DFB lasers [12]. Due to these properties, phosphate glasses have recently become appealing for optical communications [13], laser sources as well as

optical amplifiers with record values of the gain per unit [14–17] and optical parametric oscillators [18].

The main objective when developing new solid-state lasers and amplifiers is to increase the performances of the Er-doped glass such as absorption and emission cross sections, spectral shapes of the emission and absorption bands, excited state lifetimes, as well as the ion-ion interactions. It is well known that these properties are governed by the host material [1, 19]. In our previous studies, we investigated the effect of the glass composition on the physical, structural and luminescence properties of Er<sup>3+</sup> containing glasses in the system P<sub>2</sub>O<sub>5</sub> – SrO – Na<sub>2</sub>O [20] and we found that the investigated glasses possess a good thermal stability and are therefore promising for the fabrication of fiber lasers and amplifiers.

In this paper, we discuss the details of the fabrication process used to draw fibers from preforms of glasses within the P<sub>2</sub>O<sub>5</sub> – SrO – Na<sub>2</sub>O system. We assess the resulting thermal and structural properties of the fiber as compared to those of the parent preform and some spectroscopic properties of the fiber. The fiber exhibits super-broad luminescence over 70 nm obtained in just a few cm of fiber length. Additionally, the fiber exhibits spectral hole burning effect, when the fiber length exceeds 2 cm, and it is enhanced in longer fibers.

## 2. Experimental

A 25 g batch of glass with the composition 49P<sub>2</sub>O<sub>5</sub>-39.2SrO-9.8Na<sub>2</sub>O-0.5Er<sub>2</sub>O<sub>3</sub>-1.5Yb<sub>2</sub>O<sub>3</sub> (mol%) was prepared by the conventional melt-quenching technique using NaPO<sub>3</sub> (Alfa Aesar), SrCO<sub>3</sub> (Sigma-Aldrich, ≥99.9%), Er<sub>2</sub>O<sub>3</sub> (MV Laboratories Inc., 99.9%) and Yb<sub>2</sub>O<sub>3</sub> (Sigma-Aldrich, 99.9%). The Sr(PO<sub>3</sub>)<sub>2</sub> precursor was independently prepared using SrCO<sub>3</sub> and (NH<sub>4</sub>)<sub>2</sub>HPO<sub>4</sub> as raw materials and with a heating up to 850 °C. The 25 g batch was melted for 45 min at 1150°C and then casted in a 11 cm long graphite mold with a diameter of 1 cm, pre-heated at 300°C. After quenching, the preforms were annealed at 400°C for 10 hours to decrease the residual stress. Finally, the preforms were cooled down to room temperature.

Unclad monoindex fibers were drawn by “rod” method as described in [21]. To reduce the moisture concentration, the system was purged with Ar before drawing. The highest attention during the drawing process was applied to the thermal parameters. To avoid either nucleation or crystallization during the drawing, the temperature of the hot-zone and pre-heat zone was precisely mapped and the dwell time in these zones were controlled before and during the process. The fiber was drawn at 550 °C in He inert atmosphere. More than 150 m of uncoated (without any protective polymer layer) single core fibers with a diameter of (115 ± 1) μm were drawn at a rate of ~10 mm/min with a feed rate at 2 mm/min. Uncoated fibers were pulled for the measurement of the thermal, structural and optical properties of the fibers.

The structural composition of the fiber was examined by a scanning electron microscope (Carl Zeiss Crossbeam 540) equipped with Oxford Instruments X-MaxN 80 EDS detector.

The thermal properties of the glasses were measured by differential thermal analysis (Netzsch F1 JUPITER). The glass transition temperature (T<sub>g</sub>) and the crystallization temperatures (T<sub>x</sub>) were recorded at a heating rate of 10 K/min. T<sub>g</sub> was taken at the inflection point of the endotherm, as obtained by taking the first derivative of the DSC curve. The onset (T<sub>x</sub>) and the peak (T<sub>p</sub>) crystallization temperatures were taken at the onset and the highest point of first exothermic peak, respectively. All the characteristic temperatures were obtained with an accuracy of ± 3°C.

The IR spectra were measured using a ‘Perkin Elmer Spectrum one FTIR spectrometer’ in Attenuated Total Reflectance (ATR) mode in mid infrared region 600-1400 cm<sup>-1</sup>. The resolution used was 2 cm<sup>-1</sup> and the spectra were obtained from the accumulation of 8 scans.

The absorption spectrum of the fiber was measured using a stabilized broadband white light source (Thorlabs SLS201L), while the luminescence spectra were obtained under excitation of 980 nm laser diode (II-IV Laser Enterprise). The absorption and luminescence spectra were measured with resolution of 0.01 nm.

### 3. Results and discussion

As explained in [21], a glass to be considered a suitable candidate for fiber drawing, needs to exhibit a good thermo-mechanical resistance to casting (shock, fracture) and it needs to be also stable against crystallization. This resistance to crystallization is verified by measuring the glass transition temperature,  $T_g$  and the onset of the crystallization temperature,  $T_x$ . The difference between these values,  $\Delta T = T_x - T_g$ , should be as high as possible so that the glass is expected to form a fiber of good optical quality with minimal scatter loss from microcrystallites.

The thermal, structural and optical properties of the fiber were measured and compared to those of the bulk. The thermal properties of the preform and the fiber are reported in Table 1.

**Table 1. Thermal properties of the preform and of the corresponding fiber**

Sample code	$T_g$ (°C) $\pm 3^\circ\text{C}$	$T_x$ (°C) $\pm 3^\circ\text{C}$	$T_p$ (°C) $\pm 3^\circ\text{C}$	$\Delta T = (T_x - T_g)$ (°C) $\pm 6^\circ\text{C}$
Preform	462	580	593	118
Fiber	456	578	594	122

The large  $\Delta T$  value confirms the reasonable thermal stability of this glass. No significant changes in the thermal properties of the glass can be observed after drawing except for the slight decrease in  $T_g$ . Whereas the  $\Delta T$  value of the investigated glass is low compared to that of Barium Phosphate Glasses reported between 175 and 250°C [22] and to that of tellurite glasses reported at 178°C in [23], it is larger than 100°C confirming the reasonable thermal stability of this glass.

Within the accuracy of the measurement ( $\pm 1.5$  at.%), the fiber composition was found to be identical to that of the preform. Figure 1 shows a SEM image of a cross-section of a fiber. As illustrated in Fig. 1, the core is circular and concentric. No variation in the core diameter and shape has been observed when examining multiple fibers pieces.

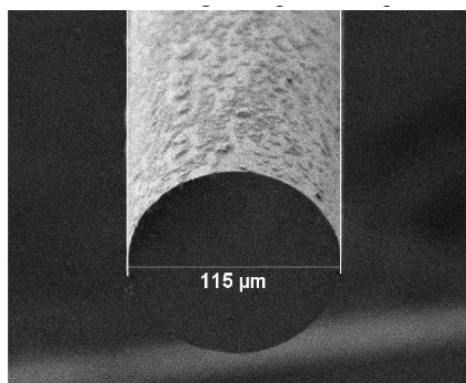


Fig. 1. SEM image of the fiber cross-section.

The impact of the fiber drawing on the glass structure was investigated using FTIR spectroscopy. Figure 2 presents the IR spectra of the glass prior to and after drawing. All spectra were normalized to the band with maximum intensity peaking at  $\sim 880$   $\text{cm}^{-1}$ . The spectra are similar to those reported in [20]. One can notice that the drawing process leads to a shift of the bands to lower wavenumber, a small increase in intensity of the band in the 700-800  $\text{cm}^{-1}$  range and a decrease in intensity of the bands at 1080 and 1250  $\text{cm}^{-1}$ . A complete

attribution of the IR bands can be found in [20, 24]. The variation in intensity and shift of the IR bands after drawing indicates that minor change in the structure of the glass occurs during fiber drawing. The decrease in intensity of the shoulder at  $980\text{ cm}^{-1}$  and of the band at  $1085\text{ cm}^{-1}$  and the small shift of band positions towards lower wavenumber after fiber drawing denotes that the fiber has weaker network connectivity and probably re-orientation of the P-O-P bonds compared to that of the bulk glass. This change in the glass structure induced by the fiber drawing process is in agreement with the reduction of  $T_g$  after drawing and might be due to severe quenching under the imposed drawing stress. Similar changes were observed during the drawing of tellurite glasses [23].

The absorption cross-section of the glass bulk at 980 and 1550 nm were estimated from the absorption coefficient at  $8.30 \cdot 10^{-21}$  and  $5.79 \cdot 10^{-21}\text{ cm}^2$ , respectively, at  $\pm 10\%$  [24]. The luminescence lifetime for  $^4I_{13/2}$  state of  $\text{Er}^{3+}$  ions was measured as  $(3.47 \pm 0.02)\text{ ms}$  [24].

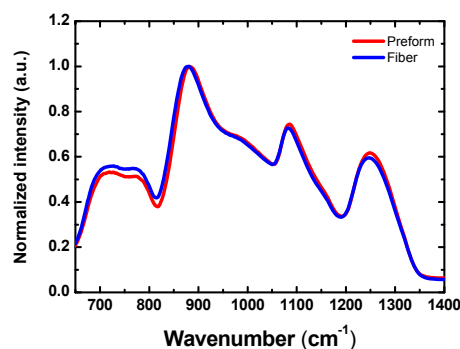


Fig. 2. IR spectrum of the preform before and after fiber drawing.

The potential performance of the light source based on erbium-glass material is determined by its emission and absorption properties, due to its three-level nature of their spectral shape and population inversion. Therefore, we investigate the optical properties of the fiber. The normalized absorption spectra of the fiber and the preform are presented in Fig. 3. The spectrum exhibits several bands, which correspond to the energy transition of  $\text{Er}^{3+}$  and  $\text{Yb}^{3+}$  ions.  $\text{Yb}^{3+}$  ions exhibit strong and sharp absorption band at a peak wavelength of 975 nm with broad absorption wing at the short wavelength side. This band is a result of energy transition between  $^2F_{7/2}$  and  $^2F_{5/2}$  energy levels. The bandwidth of the main band equals to 9.5 nm indicating poor wavelength tolerance for the pump laser. The peak absorption value at 975 nm is equal to 20 dB/cm. The broad absorption band at short wavelength side has its maximum at 950 nm and a shoulder at 928 nm. The corresponding values of absorption are 6.0 and 4.9 dB/cm. These values of absorption are weaker than at 975 nm and accounts to transitions to higher-lying sublevel in the upper manifold, which involves the emission of one or several phonons during subsequent thermalization [25]. The spectrum also contains a band centered at 1534 nm with a shoulder at 1496 nm. The signal at shorter wavelength is relatively broad and reaches the value of 2 dB/cm. In contrary the signal at 1534 nm is narrow and equals to 3.6 dB/cm. Both bands correspond to the energy transition from manifold  $^4I_{13/2}$  to  $^4I_{15/2}$ . It is evident from the figure that the absorption spectra for both the preform and the fiber are almost identical. A small shift towards the longer wavelength of the absorption bands can be observed after drawing confirming that the rare earth sites have not changed dramatically during the drawing of the fiber. The propagation losses of the fiber were estimated by the cut-back technique and do not exceed 0.2 dB/cm at 1.3  $\mu\text{m}$ .

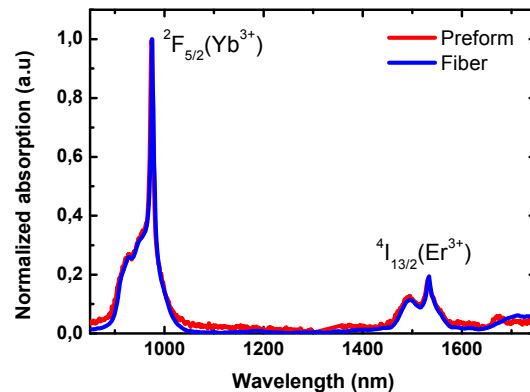


Fig. 3. Spectrum of absorption of Er/Yb-doped phosphate preform and fiber in near IR wavelength region.

The emission spectra of 1 cm long fiber were measured using a laser diode excitation at 975 nm. The obtained spectra of luminescence together with absorption spectra are presented in Fig. 4(a) and 4(b). 1 cm of the fiber length is not long enough to absorb fully the pump light, therefore, the spectrum denotes residual pump at 975 nm wavelength. The fiber exhibits at 1000 nm and 1500 nm indicating that Yb ions play dual role in the fiber: they act as activators (emitters) but also as sensitizers. The 975 nm photon is absorbed by Yb ions leading to the transition from  $^2F_{7/2}$  ground state to the  $^2F_{5/2}$  excited state. Then there are two possible scenarios. In the first scenario, the excited  $Yb^{3+}$  ions transfer, their energy to  $Er^{3+}$  ions, exciting them to the  $^4I_{11/2}$  level. The  $Er^{3+}$  ions go through non-radiative decay and as a result, the inverse distribution is formed between the  $^4I_{13/2}$  and  $^4I_{15/2}$  levels leading to emission at  $\sim 1534$  nm wavelength range. In the second scenario, Yb ions operate as efficient sensitizer without Yb-Yb interaction, when the rate of energy transfer and the lifetime of the Er-excited state are shorter than the lifetime of the Yb-excited state. The condition is satisfied at relatively moderate launched pump power or lower according to [26], or when the ratio of concentration of Er/Yb is above a certain threshold level experimentally obtained as  $\sim 4$  [27]. In our case the Er/Yb ratio is 0.3, therefore, this condition is not satisfied. Therefore, the Yb-excited state will spontaneously decay first, resulting in parasitic luminescence in the 1000 nm wavelength range. In this scenario, the excited  $Yb^{3+}$  ions go from the lowest Stark level of  $^2F_{5/2}$  manifold to sub-levels of  $^2F_{7/2}$ , and then, by means of non-radiative decay relax to the ground Stark level. This results in luminescence around 1000 nm, which is characterized by single band spectrum with central wavelength 1015 nm (Fig. 4(b)).

The absorption and emission spectra centered at  $\sim 1534$  nm are shown in Fig. 4(a). The main band of the spectra lie within 0.4 nm of each other indicating that the same pair of Stark sublevels contributes both the emission and absorption. The emission spectrum of the fiber is composed of several bands located at 1498, 1534, 1554 nm corresponding to the electronic transitions between the Stark manifolds of the excited ( $^4I_{13/2}$ ) and lower-lying energy levels of  $Er^{3+}$  ( $^4I_{15/2}$ ). The emission spectrum approaches 58 nm of bandwidth value, which is broad compared to silica fiber for examples (emission bandwidth of 35 nm as reported in [28]). This broad emission is a result of inhomogeneous broadening originating from local site-to-site variation in emitting centers' surrounding field in the lattice environment as suggested in [29].

The dependence of emission at 1000 nm and 1500 nm with pump power are presented in Fig. 4(c). The spectra clearly show the equal and simultaneous increase in emission of both Yb and Er ions with an increase in pump power. Their amplitudes increase proportionally to the pump power until initiation of saturation whereas their line shapes and bandwidths do not change. The emission at  $\sim 1000$  nm has a smaller intensity than the emission at  $\sim 1500$  nm.

With the increase of pump power, the difference between the intensity of the luminescence at 1000 nm and at 1500 nm decreases reaching the minimum difference value almost equaled to 3 dB (Fig. 4(c)). This means that the intensity of the 1000 nm luminescence raises faster with an increase in pump power than the intensity of the 1500 nm luminescence due to the domination of relaxation of Yb-excited state via spontaneous decay at higher pump rates.

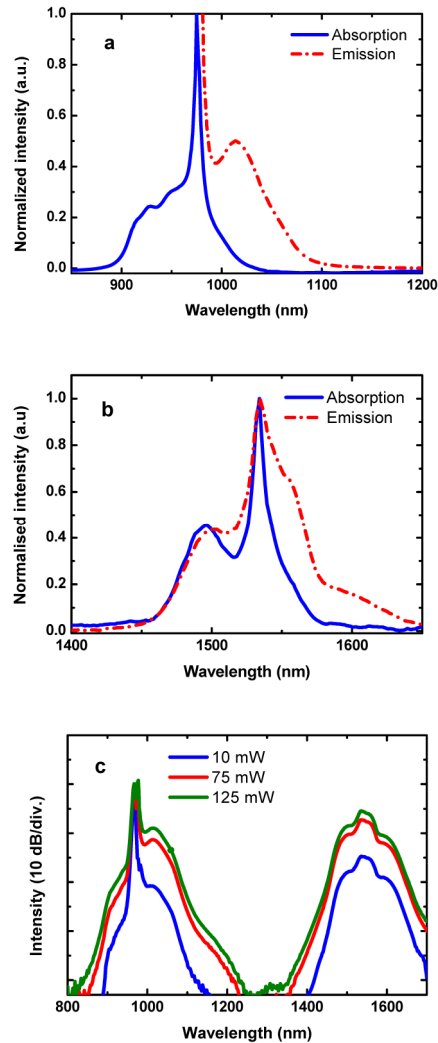


Fig. 4. Optical properties of 1 cm phosphate fiber sample. Normalized spectra of absorption and emission at 975-1100 nm (a) and 1450-1600 nm (b) wavelength ranges. c –The dependence of luminescence emission of Yb and Er ions on the pump power.

It should be noted that the phosphate fibers are characterized by higher phonon energy than silica glass [30], therefore the up-conversion emission in visible wavelength range possesses low efficiency in comparison to the down-conversion emission and is not taken into account in this study.

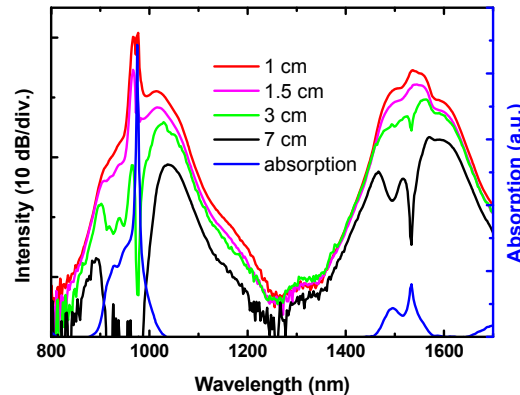


Fig. 5. Luminescence spectra for different lengths of phosphate fiber and absorption spectrum using 125 mW pump power at 975 nm.

Figure 5 shows the emission spectra of fiber with different lengths. When the fiber length increases from 1 to 7 cm, the position of the bands at  $\sim 1000$  and  $1534$  nm shifts to higher wavenumber for the fixed pump power of 125 mW. The overall shift of peak wavelength for 1000 nm band is equal to 24 nm, while for the 1534 nm band, it exceeds 35 nm. The bandwidth of the band at 1534 nm increases from 58 nm (for 1 cm) to 70 nm (for 7 cm). One can also notice that the shape of the emission bands changes due to changes in the fiber length: for long fibers (3 and 7 cm), the bands are not anymore flat and uniform, the emission bands exhibit pronounced peaks and dips, the number of which consistently increases with fiber length. These changes in the emission spectra induced by the changes in the fiber lengths are a clear sign of spectral hole burning effect as reported in [31]. These changes are due to strong reabsorption of the peak wavelength at 974 nm by  $\text{Yb}^{3+}$  ions and at 1534 nm by  $\text{Er}^{3+}$  ions originated from high concentration of the rare-earth ions ( $1.58 \cdot 10^{20} \text{ cm}^{-3}$  for Er and  $4.75 \cdot 10^{20} \text{ cm}^{-3}$  for Yb) and insufficient pump level to stimulate luminescence. Therefore, the spectra of the 3 and 7 cm long fiber look similar to inverted absorption spectrum (Fig. 5). The absorption cross-sections of Yb and Er ions in the longer wavelength is low compared to emission cross sections. Therefore, reabsorption of luminescence in this region is negligible, and consequently, it results in red shift of the central wavelength peaks. The overall drop of the spectra amplitude with an increase of the fiber length relates to the leakage of the light from the fiber due to unsatisfied requirement of total internal reflection in the unclad fiber type and can be easily eliminated by drawing new structural core-clad fiber [32].

#### 4. Conclusion

We report the results on the processing and characterization of phosphate fiber drawn from the preform prepared by standard melting process. IR spectroscopy was used to identify minor structural modification induced by the fiber drawing. These changes were attributed to modification to the bulk glass' thermal history upon drawing; the fiber is suspected to have a weaker network connectivity and probably re-orientation of the P-O-P bonds compared to that of the bulk glass in agreement with the reduction of  $T_g$  after drawing. The fiber sample exhibits propagation losses of 0.2 dB/cm and super-broad luminescence reaching the value of 70 nm just in few cm of fiber length.

This compact and broad luminescence source is useful in several demanding applications such as LIDAR or optical coherence tomography. On the other hand, the spectral hole burning effect observed in the phosphate fiber with the length exceeding 3 cm could be

interesting for ultra-high density optical data storage, processing, laser frequency stabilization, and portable frequency standards.

### **Funding**

Academy of Finland through the Competitive Funding to Strengthen University Research Profiles program (310359), for Academy project (308558) and Academy of Finland Postdoctoral research project (285170).

### **Acknowledgment**

Dr. Turkka Salminen is thanked for carrying out the SEM/EDS analysis.